Journal of Dynamics, Monitoring and Diagnostics, 2024, 3, 21-31
https://doi.org/10.37965/jdmd.2024.475

ISTP
RESEARCH ARTICLE

Investigation into Impedance Measurements for Rapid Capacity Estimation of Lithium-ion Batteries in Electric Vehicles

Xiaoyu Zhao,[1] Zuolu Wang,[1] Eric Li,[2] and Haiyan Miao[1]
[1]Centre for Efficiency and Performance Engineering, University of Huddersfield, Huddersfield, HD1 3DH, UK
[2]School of Computing, Engineering & Digital Technologies, Teesside University, Middlesbrough, TS1 3BX, UK

(Received 02 December 2023; Revised 20 December 2023; Accepted 04 January 2024; Published online 08 January 2024)

Abstract: With the dramatic increase in electric vehicles (EVs) globally, the demand for lithium-ion batteries has grown dramatically, resulting in many batteries being retired in the future. Developing a rapid and robust capacity estimation method is a challenging work to recognize the battery aging level on service and provide regroup strategy of the retied batteries in secondary use. There are still limitations on the current rapid battery capacity estimation methods, such as direct current internal resistance (DCIR) and electrochemical impedance spectroscopy (EIS), in terms of efficiency and robustness. To address the challenges, this paper proposes an improved version of DCIR, named pulse impedance technique (PIT), for rapid battery capacity estimation with more robustness. First, PIT is carried out based on the transient current excitation and dynamic voltage measurement using the high sampling frequency, in which the coherence analysis is used to guide the selection of a reliable frequency band. The battery impedance can be extracted in a wide range of frequency bands compared to the traditional DCIR method, which obtains more information on the battery capacity evaluation. Second, various statistical variables are used to extract aging features, and Pearson correlation analysis is applied to determine the highly correlated features. Then a linear regression model is developed to map the relationship between extracted features and battery capacity. To validate the performance of the proposed method, the experimental system is designed to conduct comparative studies between PIT and EIS based on the two 18650 batteries connected in series. The results reveal that the proposed PIT can provide comparative indicators to EIS, which contributes higher estimation accuracy of the proposed PIT method than EIS technology with lower time and cost.

Keywords: electric vehicles; electrochemical impedance spectroscopy; lithium-ion battery; pulse impedance technique; rapid capacity estimation

I. INTRODUCTION

The capacity estimation of lithium-ion battery is a fundamental task for the battery management system of electric vehicles (EVs) and serves as the premise for numerous indicators, including state of charge (SOC), state of health, and remaining useful life [1,2]. In addition, the retirement of a vast number of EVs poses higher capacity assessment requirements for the secondary utilization of lithium batteries [3]. The fast and accurate capacity estimation is becoming increasingly crucial for handling such a substantial quantity of batteries.

There are currently three popular methods for battery capacity estimation, which include the incremental analysis method, material properties evaluation-based method, and impedance evaluation-based method. The incremental analysis method is the most commonly adopted method due to the data availability and low-cost characteristics [4,5]. However, it requires a time-consuming step to extract capacity-related features from the long-time raw charge–discharge profile during the battery aging process [6]. Though some studies [7,8] indicate that the capacity estimation can be conducted utilizing the partial charge–discharge profile instead of the entire profile, it still demands long-duration feature extraction and requires the battery to be operated under a fixed condition to satisfy the data acquisition, which is not feasible in the real-world applications [9,10]. The material property-based evaluation method proposes to apply the ultrasonic-guided wave [11,12] and acoustic emission [13] techniques to the tested battery. Based on the echo analysis, it measures capacity-related characteristics, such as signal amplitude (SA) [14] and time of flight (ToF) [15], thereby attaining battery capacity estimation. Though the material-based method can be operated rapidly, it is still a laboratory method and has not seen the online application due to the complexity of the application environment and the challenge of interpreting the acquired echo signal.

It is believed that the impedance-based method provides a noninvasive approach to investigate battery internal electrochemical dynamics, which can reflect the battery aging mechanism [16,17]. As the active electrode materials degrade with cycling aging, the contact surface of the electrode for conducting the electrochemical reaction decreases, and it leads to the increase of both contact and charge transfer impedances [18]. The loss of lithium-ion inventory caused by aging activities, such as solid electrolyte interface (SEI) film formation and cathode electrolyte interface (CEI) formation, can lead to the blocking of the flow of ions, which brings large resistance for normal electrochemical processes [19]. As the impedance-based method can provide such informative knowledge of the battery in a nondestructive and fast manner compared to

Corresponding author: Zuolu Wang (e-mail: z.wang3@hud.ac.uk).

the incremental analysis method and material properties evaluation-based method, it is seen as the promising solution for the rapid and accurate capacity estimation of lithium-ion batteries.

Currently, the most prevalent impedance evaluation-based methods are the DCIR [20,21] and electrochemical impedance spectroscopy (EIS) [22,23] methods. To be more specific, DCIR is a resistance-based method. It imposes a one-off DC current pulse to a tested battery and acquires the voltage response. Then, the DCIR can be obtained by calculating the ratio of the changes of the two signals ($\mathrm{DCIR} = \Delta U/\Delta I$) in which ΔU and ΔI denote the difference of the voltage and the difference of the current across the battery, respectively [24]. The calculated DCIR can enable the rapid estimation of battery capacity, as the correlation has been verified between the DCIR and the capacity [20]. Gasper *et al.* [25] measured 32 cells in various capacity fading stages and generated thousands of DCIR results to verify the relationship between battery resistance and battery degradation pattern. A lot of work has been done to improve the reliability of DCIR methods. Studies in [26,27] compared the DCIR calculation performance when applying different durations of a current pulse, as some crucial electrochemical reactions, such as charge transfer and diffusion within the battery, require time to conduct. Besides, some works in [28–30] investigated and divided ΔU into many parts based on the voltage slop, aiming to link these variations directly to the internal characteristics of the battery. Instead of calculating the DCIR based on the starting edge of the pulse, some other work also [31,32] proposed to calculate the DCIR using the edge section at the relaxation when the pulse is about to be terminated and claimed it could give more reliable DCIR results with less noise caused by the measurement equipment. In addition, some studies [33–36] investigated the factors that can affect the resistance measurement, which further influences the accuracy of capacity estimation. It considered the factor of temperature and SOC to establish a look-up table of how these factors influence battery capacity estimation. The DCIR can be seen as a rapid method, and the measurement procedure is not complex, but its evaluation accuracy is a big concern in practice. Battery's internal resistance is a small value and is susceptible to measurement environment and limited information restrained by the single DC excitation component, causing unreliable test results [37].

By contrast, EIS adopts the frequency sweeping technique, and thus, it can measure the impedance response at a wide range of the frequency band from kHz to milli-Hz, which provides a large amount of information about the battery electrochemical dynamics and internal characteristics reflecting the capacity decline [38,39]. The ohmic resistance in the EIS profile is the most considered influential capacity-related feature [40,41]. Additionally, the mid-frequency information in EIS indicates solid electrolyte interface (SEI)—a side reaction product contributing to capacity fading [42]. Thus, Chang et al. [43] suggested that capacity-related features from the mid-frequency section should be further extracted. In [44], Zhou *et al.* produced novel capacity features by fitting the EIS mid-frequency section with a semicircle and applied the features to their Gaussian process regression (GPR) model. Though it introduced the extra computation cost and high workload by manually extracting features, the model showed good capacity-indicated SOH estimation performance, with most root mean squared error (RMSE) lower than 1% in considered scenarios. In addition to the mid-frequency band of EIS, Su *et al.* [45] indicated that the low-frequency band in EIS presents the diffusion process and could also be valuable in estimating the battery capacity. Their GPR model only used the low-frequency band information and attained a SOH estimation model with RMSE below 1% and R^2 above 0.95.

Since EIS includes rich and comprehensive information about battery aging, it is considered to present more reliable and accurate results in battery capacity estimation over direct current internal resistance (DCIR) [46]. However, the implementation of the EIS relies on offline specified equipment and takes much longer time than DCIR. Although EIS can provide more accurate and stable results than DCIR, it is limited to be employed as a fast and cost-effective battery capacity estimation method.

In our previous work [47], the pulse impedance technique (PIT) has been proposed to measure battery impedance in a fast manner and free from limitations of specialist equipment. The impedance calculation focuses on the dynamic responses of current and voltage transient spikes instead of static components in the conventional pulse test, which obtains more information about battery dynamics. The proposed PIT has been validated in the simulation and experiment by only distinguishing three pouch lithium batteries with different aging conditions.

However, several limitations have been identified from the previous study. First, the PIT method was only tested on a single type of battery, which raises concerns about its generalization ability across different battery chemistries. Second, the PIT was only validated on three aging samples. Such small samples are insufficient to demonstrate the reliability of the PIT on effective aging feature extraction and battery capacity estimation. Last, the lack of comparison with the well-established EIS method in our previous study makes it difficult to highlight the advantages of the PIT. Therefore, addressing the above limitations is valuable in demonstrating the reliability and generalization of the PIT.

Based on the mentioned issues, this paper investigates the above impedance-based methods for rapid and accurate capacity estimation of EV lithium-ion batteries. The EIS and PIT methods are employed to test two connected Samsung 18650 batteries in every ten aging cycles among the 1-160 cycles. Then, the impedance-based capacity-related health features are separately obtained based on the two methods. Afterward, various impedance features and statistical features are analyzed, from which the health features strongly related to the capacity decline in both methods are identified with the Pearson correlation analysis. Next, we develop linear regression models to map the relationship between the features extracted from the two methods and the actual capacity. A comparative study of the model's fitting performance is performed accordingly, in which both PIT and EIS are evaluated in terms of R-score and RMSE. The results indicate that the PIT method can provide informative and comparative health features compared to those from the EIS, and it can achieve more accurate battery capacity estimation with higher efficiency and lower cost.

The remainder of this paper is organized as follows: Section II demonstrates the investigated rapid battery capacity estimation technologies. Section III introduces the experimental design and implementation for two estimation technologies. Section IV displays the results and

compares two impedance-based methods for capacity estimation. Finally, conclusions are given in Section V.

II. METHODOLOGIES

The theoretical backgrounds and operational procedures of the proposed PIT and EIS measurements are demonstrated in the following sections.

A. PULSE IMPEDANCE TECHNIQUE (PIT)

PIT is a fast and low-cost impedance-based method used for battery capacity estimation. It relies on a transient signal from the pulse generated by a battery management system. Instead of using the static component in the conventional method, it captures rich aging information by analyzing the dynamic component of the response and calculating the impedance in a range of frequencies. In addition, a high sampling frequency will be used to sufficiently capture the transient information in a short time period so that the battery impedance can be calculated rapidly and accurately.

As displayed in Fig. 1(a), a pulse-based transient current signal $i(t)$ with multiple frequency components is first excited to the tested battery, and the voltage response $v(t)$ across the battery will be recorded simultaneously, as listed in Equations (1) and (2). To obtain the frequency components of the signals, we transform the raw signals to frequency domain using the fast Fourier transform separately, then the signals in frequency domain of $I(f)$ and $V(f)$ are obtained accordingly, as shown in Fig. 1(b).

$$i(t) = i_{DC} + \sum_{k=1}^{n} I_k sin(2\pi f_k t) \tag{1}$$

$$v(t) = v_{DC} + \sum_{k=1}^{n} V_k sin(2\pi f_k t) \tag{2}$$

From Equations (1) and (2), both the current and voltage signal consist of direct current (DC) and alternative current (AC) components, where i_{DC} and v_{DC} are the direct current bias for current and voltage signal, respectively. I_k and V_k are the amplitudes of the corresponding frequency f_k in the current and voltage, and n denotes the number of frequency components. Next, the coherence analysis is conducted on the signals as given in Fig. 1(c). Equations (3)–(5) are used to calculate the coherence $C_{xy}(f)$. It indicates that the band of approx. 0–200 Hz exhibits a high degree of coherence. The high coherence demonstrates the strong correlation of two signals, which suggests that two signals are synchronized and reliable for the impedance calculation. It calculates the impedance $Z(f)$ in the specified frequency band with high coherence based on Equation (6), as displayed in Fig. 1(d).

$$G_{XY}(f) = V(f)\ I(f)^* \tag{3}$$

$$G_{XXYY}(f) = I(f)\ I(f)^*\ V(f)\ V(f)^* \tag{4}$$

$$C_{XY}(f) = \frac{\left|G_{XY}(f)\right|^2}{G_{XXYY}(f)} \tag{5}$$

$$Z(f) = \frac{V(f)}{I(f)} \tag{6}$$

where $V(f)$ and $I(f)$ are the Fourier transform of the signal $i(t)$ and $v(t)$, while the $I(f)^*$and $V(f)^*$ are the conjugate of

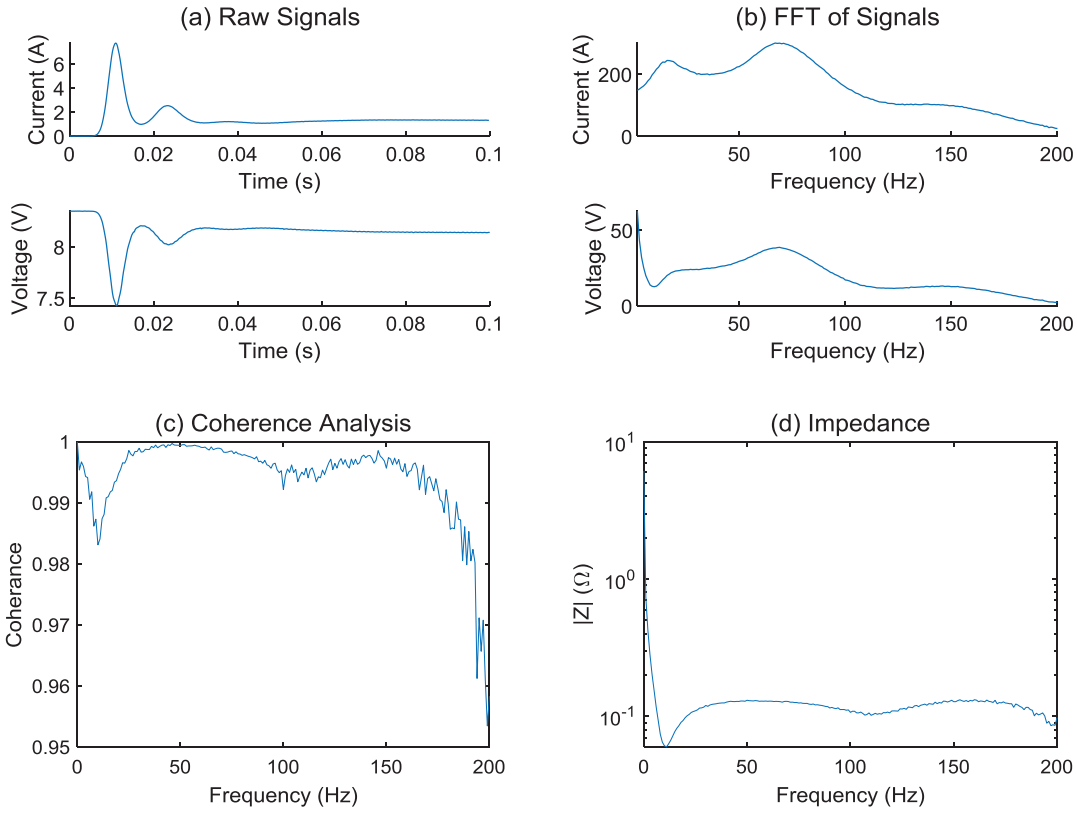

Fig. 1. The impedance-based method of PIT: (a) the raw signal of excitation and response, (b) the FFT of the signals, (c) coherence examination of the signals, and (d) impedance calculation.

$I(f)$ and $V(f)$, respectively. $G_{xy}(f)$ denotes the cross-power spectral density of the two signals, and $G_{XXYY}(f)$ is the product of the auto spectral density.

Finally, the highly efficient aging features are identified and examined by Pearson correlation analysis, as Pearson correlation analysis is valuable in identifying linear features. The identified features are suitable for developing the linear model to estimate the battery capacity. The Equation (7) displays the Pearson coefficient calculation.

$$\rho = \frac{\sum_{i=1}^{N}(x_i - \bar{x})(y_i - \bar{y})}{\sqrt{\sum_{i=1}^{N}(x_i - \bar{x})^2}\sqrt{\sum_{i=1}^{N}(y_i - \bar{y})^2}} \tag{7}$$

where N denotes the number of samples from x and y, from which x and y are used to denote the extracted features and capacity, respectively.

B. ELECTROCHEMICAL IMPEDANCE SPECTROSCOPY (EIS)

Electrochemical impedance spectroscopy (EIS) is an informative method for impedance measurement, relying on multi-times tests and costly offline test system. It obtains a wide range of impedance information by sending small signals in various frequencies successively and acquiring the response, which can be used for battery capacity estimation.

In the EIS test procedure, a sinusoidal wave signal in a specific frequency is first applied as an excitation to the tested battery. The voltage response is acquired simultaneously. Second, the impedance in the specified frequency is calculated in accordance with the excitation and response. Then, it repeats the first two steps by changing the excitation frequency and sweeps in a wide frequency band. Finally, the EIS that comprises impedances in tens of frequencies is obtained from which valuable features can be identified and used for battery capacity estimation. The EIS impedance is calculated as follows:

$$i(t) = I_k sin(2\pi f_k t) \tag{8}$$

$$v(t) = V_k \sin(2\pi f_k t + \varnothing_k) \tag{9}$$

$$Z(f_k) = \frac{V_k}{I_k} e^{j\varnothing_k} \tag{10}$$

where $i(t)$is the sinusoidal current used to test the battery at frequency f_k, $v(t)$ denotes the voltage response across the battery with the phase of $\varnothing_k$ and amplitude of I_k and V_k, and $Z(f_k)$ stands for the impedance at a specified frequency.

III. EXPERIMENT

A. EXPERIMENTAL PLATFORM

An experimental platform is designed to examine the two impedance-based methods (PIT and EIS) for battery capacity estimation, as displayed in Fig. 2. The tested two

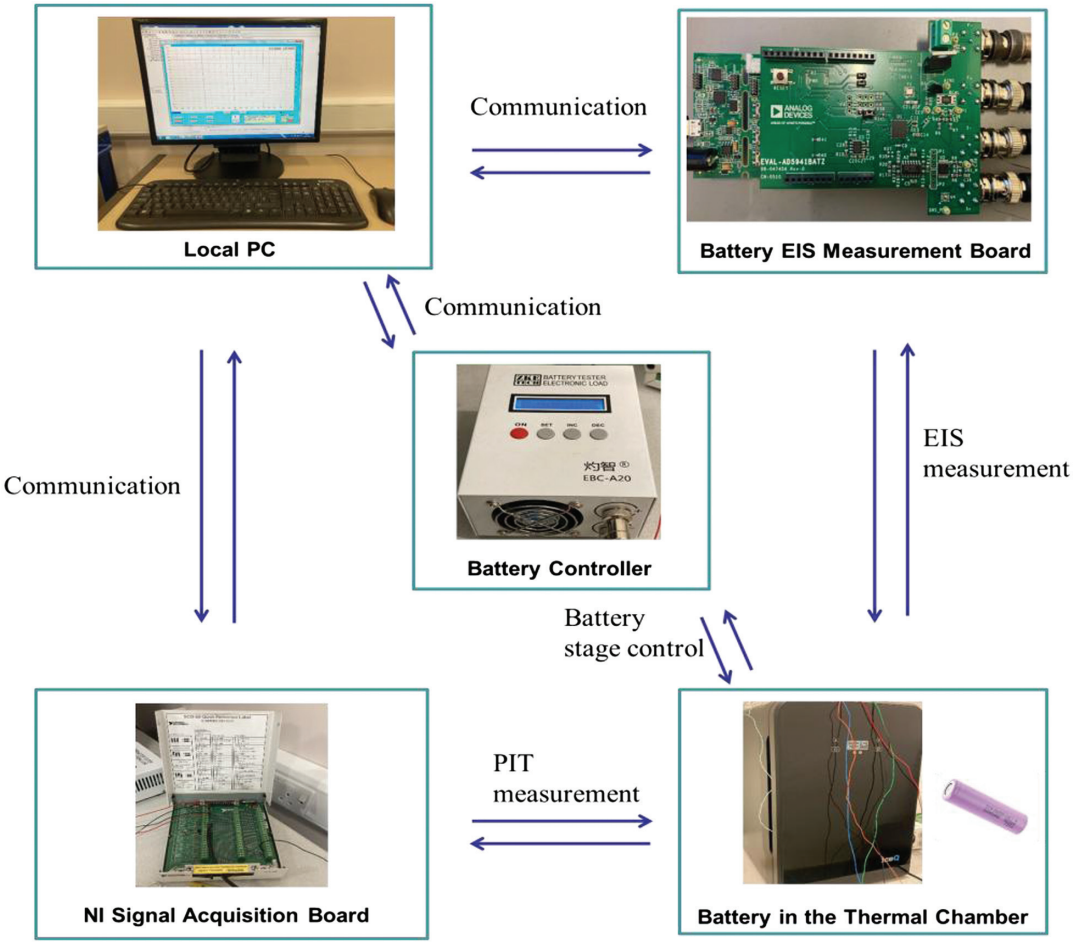

Fig. 2. The developed experimental system.

Table I. The specification of the tested batteries

Parameters	Description
Type	Samsung 18650 lithium battery
Voltage	2.75–4.2V (Nominal 3.7V)
Capacity	2.6Ah

batteries are connected in series and placed in a thermostat to be controlled at an ambient temperature. Table I displays the critical parameters of the objected battery. The battery controller is connected to the tested cells to control the battery operated in the required stages, including the charge, relaxation, and discharge stages. Moreover, the controller can measure and record the voltage and current across the battery with a low sampling rate of 0.5 Hz, and it is used to calibrate battery capacity for obtaining the battery degradation conditions. The controller, NI acquisition board, and EIS measurement board are all connected to the local PC for centralized control and data acquisition through the equipped software. The NI signal acquisition board is used for the PIT test for capturing the transient variance of voltage and current, and the EIS board is responsible for EIS measurement.

B. EXPERIMENTAL SETUP

Four groups of experiments were conducted, which were battery aging experiments, capacity calibration, PIT measurement, and EIS measurement. The aging experiments generate batteries in various aging conditions. Capacity calibration is to obtain the actual capacity value of the battery at different aging conditions, which will be taken as the output of the developed model. PIT and EIS measurements are used to obtain PIT and EIS impedances of batteries at multiple aging conditions, respectively. These impedances from the two measurement methods will be considered as input of the model for evaluating the actual capacity of the battery. The following gives the details for the setups of each experiment:

1) AGING EXPERIMENT. It sets battery controller for controlling the batteries at 1C (2.6A) charging rate, 2C discharging rate, and 20 min relaxation time between the switch of charge–discharge operation. The total experiments were conducted for 160 aging cycles.

2) CAPACITY CALIBRATION. It discharged the batteries from an SOC of 100% to an SOC of 0% at a 0.5 C discharging rate, from which the total amount of capacity released in this procedure by the batteries was recorded by the battery controller. After the end of every 10-cycle aging experiment, capacity calibration was conducted, and a total of 17 capacities denoting different aging conditions (including the original condition) were recorded.

3) PIT MEASUREMENT. In every ten cycles of the aging experiment, PIT measurement was conducted. First, it charged the batteries to a full charge till 8.4 V using the controller. Second, resting for 1 hour is used to ensure the batteries reach a stable state. Then, it injected a 0.5C-current pulse lasting less than 1 second into the battery and simultaneously recorded its transient current and response voltage at a fixed sampling rate of 5 kHz using the NI acquisition board. This high sampling rate can make sure that the transient information can be captured, and the battery impedance can be calculated accurately.

4) EIS MEASUREMENT. EIS measurement was also conducted in every ten aging cycles. Similar to PIT measurement, it first fully charged two cells to 8.4 V with the controller to keep the same test condition before resting for 1 hour in EIS. Then, the EIS board conducted the impedance measurement on the tested cells. The sweeping frequency range was set between 1 Hz and 1 kHz with 300 mA current excitation, and the total sampling points were 59.

It should be noted that the temperature was set to be distinct between the aging experiment and the other three experiments. To accelerate the aging process, the batteries were cycled at a higher temperature of 40°C within the highest safety operating temperature of 45°C, while the temperature was set as 25°C in capacity calibration, PIT measurement, and EIS measurement experiments.

IV. RESULTS AND DISCUSSION

A. IMPEDANCE MEASUREMENT RESULTS

The impedance measurement results of the proposed PIT and the conventional EIS methods among 160 ageing cycles are separately displayed in Fig. 3. The operational time of PIT is within one second, while it takes over 30 minutes for EIS measurement at each cycle. Specifically, in PIT, we exhibit a frequency band of 0 Hz to 200 Hz with a verified high coherence, as demonstrated in Section II, from which the band of 20 Hz to 180 Hz gives stable coherence performance and will be used for feature extraction. In EIS measurement, it considers a wide frequency band and uses a

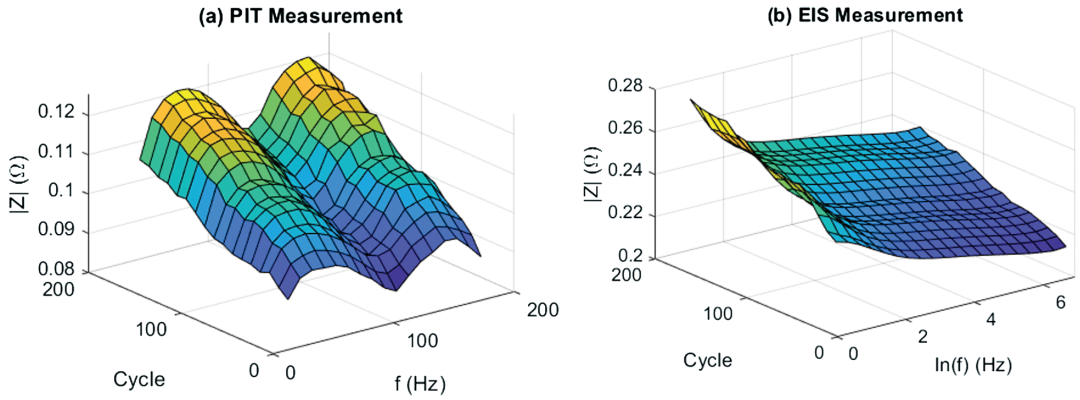

Fig. 3. The measured impedance results by the proposed (a) PIT and the traditional and (b) EIS.

specific sweeping technique that only sweeps in every decade. Thus, we take $ln(f)$ as the X-axis to give an overlook of the results.

B. FEATURE EXTRACTION

Based on the observed impedance results, we conduct feature extraction to identify the capacity-related features. Here, we consider rough features, including two categories of directive features and statistical features. The following gives the details of the two types of features:

Directive Feature: These features are the amplitude of impedance at a fixed frequency. Since PIT and EIS methods evaluate battery aging conditions in different ranges of frequency bands, the number of features that can be extracted from two methods is distinct. It only considers the band of 20–180 Hz at an interval of 10 Hz in PIT, the total impedance that can be obtained is 17. In EIS, it generates 59 frequencies, and we obtain 59 impedances accordingly.

Statistical Feature: Various statistical features, including variance (var), standard deviation (std), coefficient of variance (cv), mean, maxima (max), and minima (min), are used to analyze the battery impedance. The statistical features extracted from PIT and EIS are separately displayed in Figs. 4 and 5. In Fig. 4(a, b), the *var* and *std* present an increasing trend with battery capacity decline, indicating a more considerable variation of impedance from different frequencies as the battery ages in PIT. However, this trend

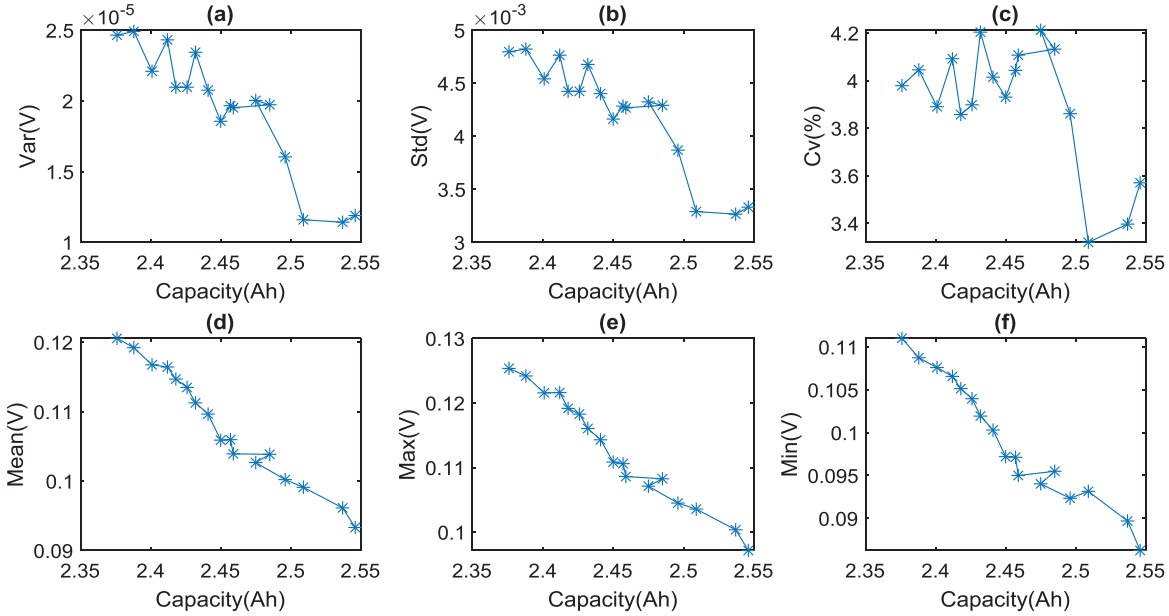

Fig. 4. Statistical features of (a) var, (b) std, (c) cv, (d) mean, (e) max, and (f) min extracted from PIT.

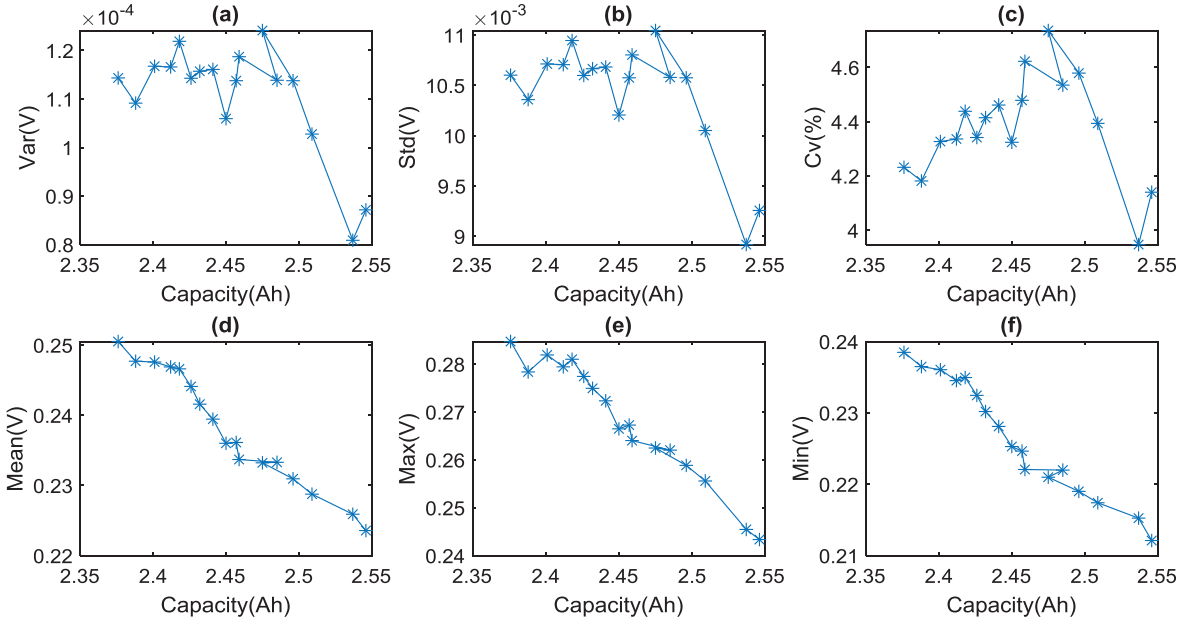

Fig. 5. Statistical features of (a) var, (b) std, (c) cv, (d) mean, (e) max, and (f) min extracted from EIS.

is not apparent in EIS, as shown in Fig. 5(a, b). In addition, it can be seen from Figs. 4(d–f) and 5(d–f) that the extracted statistical features, such as *mean, max*, and *min*, from both PIT and EIS are closely related to the capacity change. Based on the results, we notice that some features, such as *cv* in both methods (see Figs. 4(e) and 5(e)) and *var* in EIS, do not present a strong correlation with the aging pattern.

Pearson analysis is valuable in identifying linear features, and these features are suitable for developing the linear model to explore the mapping relationship between the identified feature and capacity. Despite some features displaying correlated variations with the capacity, the relationship is not linearly correlated, such as *var* in PIT, as shown in Fig. 4(a), which will affect the linear model's estimation performance. Accordingly, we adopt Pearson correlation analysis to further examine these rough features to obtain the optimal life-related feature for the final capacity estimation.

The Pearson analysis results are displayed in Fig. 6, where *fi* is used to denote impedance features obtained at a specific frequency, and *cap* is short for the capacity. Due to the space limits and similar performance of adjacent impedances, it only exhibits the coefficient of five representative impedances of PIT and EIS at a fixed interval of samples. The intervals of the adjacent impedance samples are 3 and 12 for PIT and EIS, respectively. Table II lists the corresponding frequencies indicated by the evaluated features in both methods.

Table II. The actual frequency (Hz) of the representative features in both methods

Method	*f1*	*f2*	*f3*	*f4*	*f5*
PIT	30	60	90	120	150
EIS	1.12	4.58	18.67	76.10	310.12

Figure 6 separately exhibits the Pearson coefficient between directive impedance features and capacity, statistical features, and capacity in PIT and EIS methods. As shown in Fig. 6(a), in PIT method, most features can be found with a coefficient higher than 0.98, such as *f2* and *f5*, which indicate excellent health indicators that can be used for battery capacity estimation. Moreover, the founded highly correlated features of *f1 f2*, *f3*, and *f5* are strongly related to each other with an absolute value of more than 0.99. This demonstrates that only a single health feature can give a comprehensive expression of these features. Hence, we select *f2* in PIT as the optimal impedance feature. Similarly, the health feature extraction is conducted in EIS. As shown in Fig. 6(b), the *f3* is chosen as the optimal health feature in EIS due to its high correlation with capacity and the other features. As displayed in Fig. 6(c, d), the Pearson correlation of statistical features

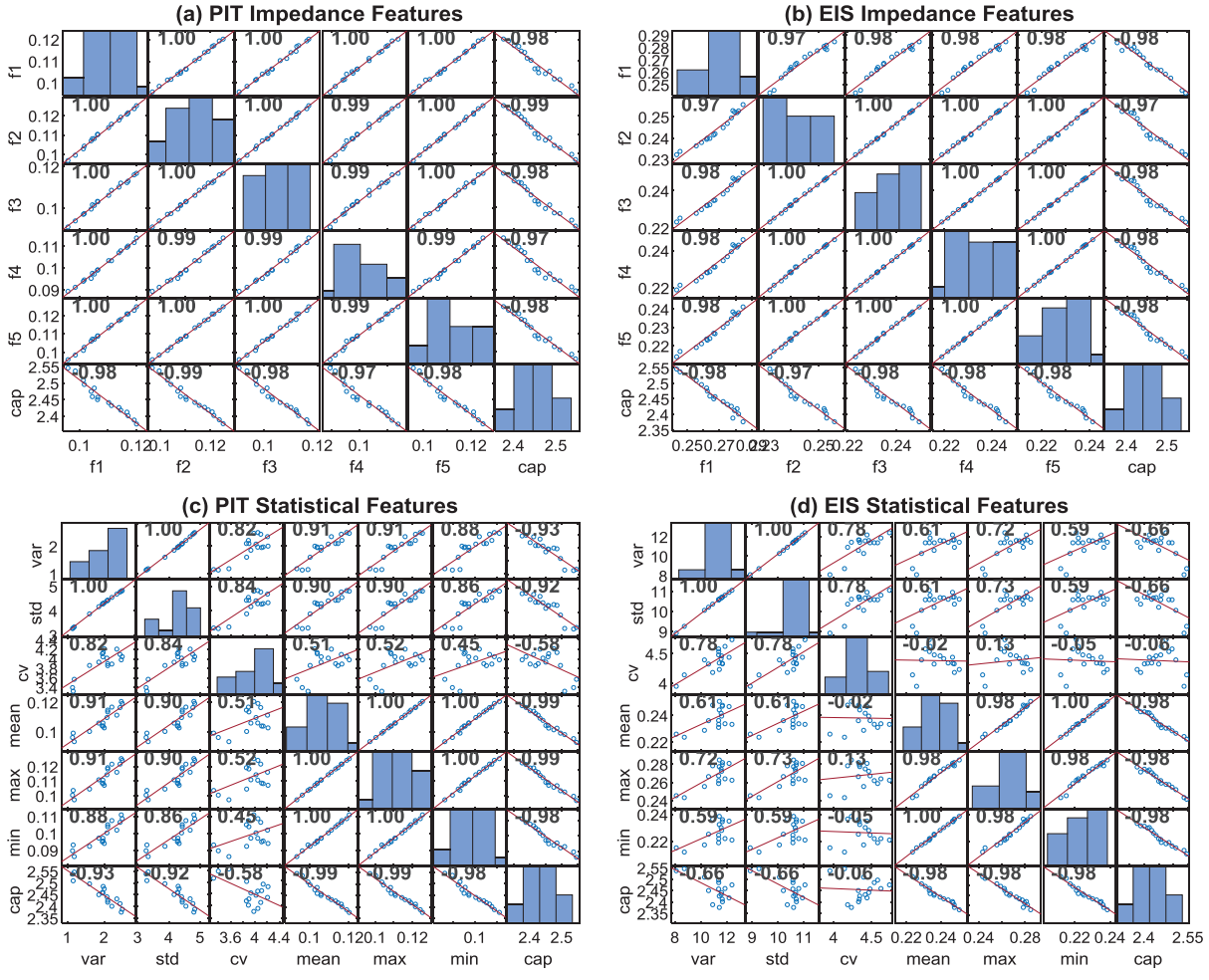

Fig. 6. The Pearson correlation analysis of impedance features from (a) PIT and (b) EIS and statistical features from (c) PIT and (d) EIS.

from PIT and EIS is examined, respectively. Some statistical features, such as *cv*, show less correlation with the capacity change. Nevertheless, it still identifies some valuable life-related statistical features from PIT and EIS, such as *mean* and *max*. Though we found *var* and *std* features, which have a coefficient higher than 0.9 in PIT, they are not chosen as the optimal feature, as their correlation performance is not as strong as that of *max*. Also, *max* is the most related feature to the other statistical features. Thus, *max* is taken as the representative statistical feature for both methods.

Meanwhile, we can conclude that conducting Pearson correlation analysis is meaningful, as it can avoid taking a non-related impedance as the health indicator, reducing data dimension and model's complexity, and identifying the highly valuable and representative features.

C. BATTERY CAPACITY ESTIMATION

In this section, we develop linear regression models using the health feature separately extracted from the two methods to describe the capacity loss. As mentioned above, *f2* and *max* features are regarded as the representative health indicators in PIT, and *f3* and *max* are considered in EIS. We consider three scenarios, that is, utilizing the representative impedance feature, the representative statistical feature, and both features in model development. Thereby, multiple models are developed using distinct features obtained in various techniques. By comparing these models' performance, we can comprehensively compare PIT and EIS methods.

The battery capacity estimation by the linear regression model using distinct health features extracted from the PIT and EIS methods are shown in Fig. 7, and the numerical

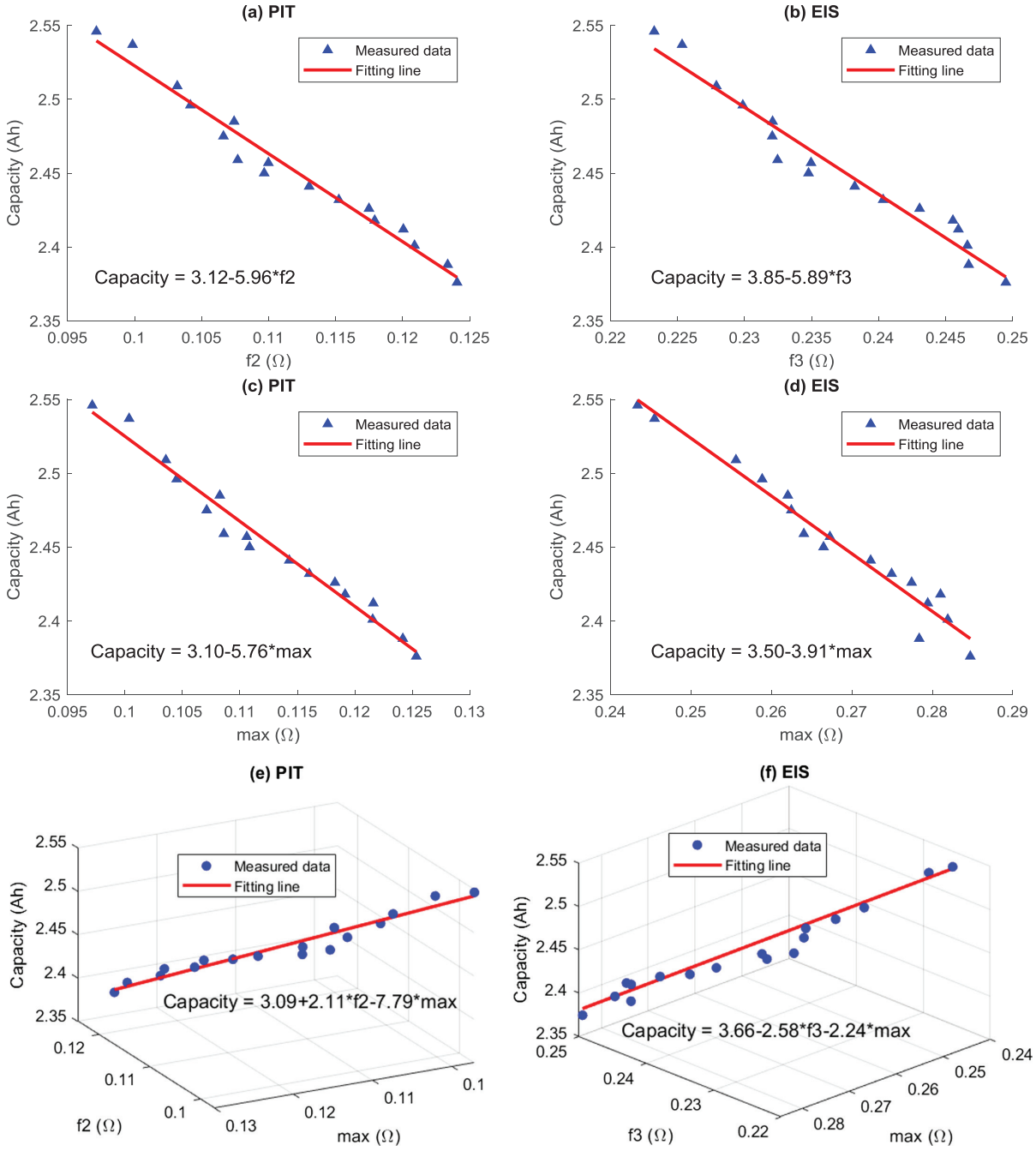

Fig. 7. The fitting performance of the model with distinct representative features from the two methods. (a) *f2* from PIT, (b) *f3* from EIS, (c) *max* from PIT, (d) *max* from EIS, (e) *f2* and *max* from PIT, and (f) *f3* and *max* from EIS.

Table III. Numerical metrics of the fitting results by the linear model with features extracted from PIT and EIS methods

Method	Features	R-score	RMSE (%)
PIT	*f2*	0.971	0.87
	max	0.973	0.84
	f2+max	0.973	0.87
EIS	*f3*	0.955	1.08
	max	0.961	1.02
	f3+max	0.968	0.94

performance of these linear models is listed in Table III. It can be noted that these models developed in extracted health features selected in both methods show a good fitting performance with the actual value. This is also verified by the evaluation metric of R-score, which shows a value greater than 0.95 in all the fitting cases. Especially, the R-score of up to 0.973 when utilizing PIT features exhibits a higher fitting result given by PIT for capacity estimation over the EIS. Moreover, the RMSE of PIT is lower at 0.87%, presenting a more reliable and accurate capacity estimation performance compared to EIS, which has an RMSE of up to 1.08%.

Overall, the results show that developing the linear model with the PIT feature can give a closer fit to the actual capacity values and yield lower errors than using EIS features in considered scenarios, demonstrating that the PIT method leads to better battery capacity evaluation performance regarding accuracy than the EIS method.

While PIT offers a good performance in battery capacity estimation, we acknowledge some limitations of this study. First, our experimental design only considers the series connection and not considers parallel connection, which may raise concerns about the effect on different connection on the method's performance. Second, the frequency component of the excitation relies on the battery controller system, which may influence the generalization of PIT method. These limitations highlight the area for future study to broaden the practical application.

V. CONCLUSION

This paper investigates two impedance measurement methods of the novel transient signal-based PIT and the conventional EIS methods for capacity estimation in the multi-batteries-connected scenario. To conduct the investigation, the PIT and EIS operations, along with the capacity calibration of the cell, are conducted on a two-battery cell with multiple levels of degradation. The measured impedance features and six statistical features of the impedance values in both methods are taken as the potential indicator and then examined by Pearson correlation analysis to identify the highly representative health features. Afterward, we developed the linear feature-capacity mapping models utilizing the extracted highly influential features from the two methods separately. Several conclusions can be summarized that the impedance-based methods of PIT and EIS can both find compelling features indicating battery capacity decline. The transient signal-based PIT is on par with the EIS method regarding health-related feature extraction, as both methods can extract influential features with Pearson coefficient higher than 0.98. Furthermore, by comparing the model's fitting results with the actual capacity, it noticed that leveraging the feature from PIT can build linear models with better performance over the one built on the EIS feature, as indicated by the higher R-score of up to 0.973 and an RMSE below 0.87%. Meanwhile, the PIT can be implemented superfast within one second, compared to the EIS, which needs over 30 minutes. Overall, PIT is preferable in battery capacity estimation regarding accuracy and efficiency and has more substantial potential for practical applications.

Future work will consider other types of lithium-ion batteries and more practical application scenarios, e.g., connected to an EV battery pack, and we will compare the PIT and EIS methods in these complex scenarios for battery capacity estimation.

ACKNOWLEDGMENTS

The authors would like to express their appreciation to the Centre for Efficiency and Performance Engineering (CEPE) at the University of Huddersfield for supporting the studies under the supervision of Professor Fengshou Gu and Andrew Ball. Additionally, the author would like to express the appreciation to the support from the China Scholarship Council (Grant No. 202108890044).

CONFLICT OF INTEREST STATEMENT

The authors declare no conflicts of interest.

REFERENCES

[1] Z. Wang, X. Zhao, L. Fu, D. Zhen, F. Gu, and A. D. Ball, "A review on rapid state of health estimation of lithium-ion batteries in electric vehicles," *Sustain. Energy Technol. Assess.*, vol. 60, p. 1, 2023.

[2] P. Makeen, H. A. Ghali, S. Memon, and F. Duan, "Electric vehicles lithium-polymer ion battery dynamic behaviour charging identification and modelling scheme," *J. Dyn. Monit. Diagn.*, vol. 2, no. 3, pp. 170–11, 2023.

[3] Z. Wang, G. Feng, X. Liu, F. Gu, and A. Ball, "A novel method of parameter identification and state of charge estimation for lithium-ion battery energy storage system," *J. Storage Mater.*, vol. 49, p. 104124, 2022.

[4] S. Shen, M. Sadoughi, X. Chen, M. Hong, and C. Hu, "A deep learning method for on-line capacity estimation of lithium-ion batteries," *J. Storage Mater.*, vol. 25, p. 100817, 2019.

[5] W. Li, N. Sengupta, P. Dechent, D. Howey, A. Annaswamy, and D. U. Sauer, "On-line capacity estimation of lithium-ion batteries with deep long short-term memory networks," *J. Power Sources*, vol. 482, p. 228863, 2021.

[6] X. Hu, L. Xu, X. Lin, and M. Pecht, "Battery lifetime prognostics," *Joule*, vol. 4, no. 2, pp. 310–346, 2020.

[7] J. Tian, R. Xiong, W. Shen, J. Lu, and F. Sun, "Flexible battery state of health and state of charge estimation using partial charging data and deep learning," *Energy Storage Mater.*, vol. 51, pp. 372–381, 2022.

[8] Y. Ni, J. Xu, C. Zhu, H. Zhang, Y. Yu, K. Song, and C. Wu, "Rapid estimation of residual capacity for retired LiFePO4 batteries using voltage interval at low state of charge," *Energy Storage Mater.*, vol. 55, pp. 463–478, 2023.

[9] G. Fan and X. Zhang, "Battery capacity estimation using 10-second relaxation voltage and a convolutional neural network," *Appl. Energy*, vol. 330, p. 120308, 2023.

[10] B. Jiang, Y. Zhu, J. Zhu, X. Wei, and H. Dai, "An adaptive capacity estimation approach for lithium-ion battery using 10-min relaxation voltage within high state of charge range," *Energy*, vol. 263, p. 125802, 2023.

[11] Z. Wang, G. Feng, D. Zhen, F. Gu, and A. Ball, "A review on on-line state of charge and state of health estimation for lithium-ion batteries in electric vehicles," *Energy Rep.*, vol. 7, pp. 5141–5161, 2021.

[12] Y. Wu, Y. Wang, W. K. Yung, and M. Pecht, "Ultrasonic health monitoring of lithium-ion batteries," *Electronics*, vol. 8, no. 7, p. 751, 2019.

[13] Z. Wang, X. Zhao, H. Zhang, D. Zhen, F. Gu, and A. Ball, "Active acoustic emission sensing for fast co-estimation of state of charge and state of health of the lithium-ion battery," *J. Energy Storage*, vol. 64, p. 107192, 2023.

[14] J. Y. Kim, J. H. Jo, and J. W. Byeon, "Ultrasonic monitoring performance degradation of lithium ion battery," *Microelectron. Reliab.*, vol. 114, p. 113859, 2020.

[15] P. Ladpli, F. Kopsaftopoulos, and F. K. Chang, "Estimating state of charge and health of lithium-ion batteries with guided waves using built-in piezoelectric sensors/actuators," *J. Power Sources*, vol. 384, pp. 342–354, 2018.

[16] D. Andre, M. Meiler, K. Steiner, C. Wimmer, T. Soczka-Guth, and D. U. Sauer, "Characterization of high-power lithium-ion batteries by electrochemical impedance spectroscopy. I. Experimental investigation," *J. Power Sources*, vol. 196, no. 12, pp. 5334–5341, 2011.

[17] W. Hu, Y. Peng, Y. Wei, and Y. Yang, "Application of electrochemical impedance spectroscopy to degradation and aging research of lithium-ion batteries," *J. Phys. Chem. C*, vol. 127, no. 9, pp. 4465–4495, 2023.

[18] C. R. Birkl, M. R. Roberts, E. McTurk, P. G. Bruce, and D. A. Howey, "Degradation diagnostics for lithium ion cells," *J. Power Sources*, vol. 341, pp. 373–386, 2017.

[19] X. Han, L. Lu, Y. Zheng, X. Feng, Z. Li, J. Li, and M. Ouyang, "A review on the key issues of the lithium ion battery degradation among the whole life cycle," *ETransportation*, vol. 1, p. 100005, 2019.

[20] E. Braco, I. San Martín, P. Sanchis, and A. Ursúa, "Fast capacity and internal resistance estimation method for second-life batteries from electric vehicles," *Appl. Energy*, vol. 329, p. 120235, 2023.

[21] J. Kim, L. Krueger, and J. Kowal, "On-line state-of-health estimation of Lithium-ion battery cells using frequency excitation," *J. Energy Storage*, vol. 32, p. 101841, 2020.

[22] B. Jiang, J. Zhu, X. Wang, X. Wei, W. Shang, and H. Dai, "A comparative study of different features extracted from electrochemical impedance spectroscopy in state of health estimation for lithium-ion batteries," *Appl. Energy*, vol. 322, p. 119502, 2022.

[23] F. Luo, H. Huang, L. Ni, and T. Li, "Rapid prediction of the state of health of retired power batteries based on electrochemical impedance spectroscopy," *J. Energy Storage*, vol. 41, p. 102866, 2021.

[24] G. Giordano, V. Klass, M. Behm, G. Lindbergh, and J. Sjöberg, "Model-based lithium-ion battery resistance estimation from electric vehicle operating data," *IEEE Trans. Veh. Technol.*, vol. 67, no. 5, pp. 3720–3728, 2018.

[25] P. Gasper, A. Schiek, K. Smith, Y. Shimonishi, and S. Yoshida, "Predicting battery capacity from impedance at varying temperature and state of charge using machine learning," *Cell Rep. Phys. Sci.*, vol. 3, no. 12, p. 101184, 2022.

[26] W. Choi, H. C. Shin, J. M. Kim, J. Y. Choi, and W. S. Yoon, "Modeling and applications of electrochemical impedance spectroscopy (EIS) for lithium-ion batteries," *J. Electrochem. Sci. Technol.*, vol. 11, no. 1, pp. 1–13, 2020.

[27] W. Waag, S. Käbitz, and D. U. Sauer, "Application-specific parameterization of reduced order equivalent circuit battery models for improved accuracy at dynamic load," *Measurements*, vol. 46, no. 10, pp. 4085–4093, 2013.

[28] V. Knap, D. I. Stroe, R. Teodorescu, M. Swierczynski, and T. Stanciu, "Comparison of parametrization techniques for an electrical circuit model of Lithium-Sulfur batteries," in *2015 IEEE 13th Int. Conf. Ind. Inf. (INDIN)*, Piscataway, NJ: IEEE, July 2015, pp. 1278–1283.

[29] A. Barai, K. Uddin, W. D. Widanage, A. McGordon, and P. Jennings, "A study of the influence of measurement timescale on internal resistance characterisation methodologies for lithium-ion cells," *Sci. Rep.*, vol. 8, no. 1, pp. 1–13, 2018.

[30] L. Wildfeuer, N. Wassiliadis, C. Reiter, M. Baumann, and M. Lienkamp, "Experimental characterization of Li-ion battery resistance at the cell, module and pack level," in *2019 Fourteenth Int. Conf. Ecol. Veh. Renew. Energies (EVER)*, Piscataway, NJ: IEEE, May 2019, pp. 1–12.

[31] W. Waag, S. Käbitz, and D. U. Sauer, "Experimental investigation of the lithium-ion battery impedance characteristic at various conditions and aging states and its influence on the application," *Appl. Energy*, vol. 102, pp. 885–897, 2013.

[32] N. Shamim, V. V. Viswanathan, E. C. Thomsen, G. Li, D. M. Reed, and V. L. Sprenkle, "Valve regulated lead acid battery evaluation under peak shaving and frequency regulation duty cycles," *Energies*, vol. 15, no. 9, p. 3389, 2022.

[33] S. J. Kwon, S. E. Lee, J. H. Lim, J. Choi, and J. Kim, "Performance and life degradation characteristics analysis of NCM LIB for BESS," *Electronics*, vol. 7, no. 12, p. 406, 2018.

[34] P. Vadhva, J. Hu, M. J. Johnson, R. Stocker, M. Braglia, D. J. Brett, and A. J. Rettie, "Electrochemical impedance spectroscopy for all-solid-state batteries: theory, methods and future outlook," *ChemElectroChem*, vol. 8, p. 11, pp. 1930–1947, 2021.

[35] Y. Troxler et al., "The effect of thermal gradients on the performance of lithium-ion batteries," *J. Power Sources*, vol. 247, pp. 1018–1025, 2014.

[36] H. Zhao, S. Wang, H. Cheng, K. Dong, and W. Liu, "Electrochemical performance of LiAlCl4/SOCl2 electrolyte with 2, 2'-bipyridine in Li/SOCl2 batteries," *Int. J. Electrochem. Sci.*, vol. 8, p. 9752, 2013.

[37] N. Meddings et al., "Application of electrochemical impedance spectroscopy to commercial Li-ion cells: a review," *J. Power Sources*, vol. 480, p. 228742, 2020.

[38] L. A. Middlemiss, A. J. Rennie, R. Sayers, and A. R. West, "Characterisation of batteries by electrochemical impedance spectroscopy," *Energy Rep.*, vol. 6, pp. 232–241, 2020.

[39] K. Mc Carthy, H. Gullapalli, and T. Kennedy, "Online state of health estimation of Li-ion polymer batteries using real time impedance measurements," *Appl. Energy*, vol. 307, p. 118210, 2022.

[40] X. Zhang et al., "Electrochemical impedance spectroscopy study of lithium-ion capacitors: Modeling and capacity fading mechanism," *J. Power Sources*, vol. 488, p. 229454, 2021.

[41] J. Wang et al., "High-efficient prediction of state of health for lithium-ion battery based on AC impedance feature tuned with Gaussian process regression," *J. Power Sources*, vol. 561, p. 232737, 2023.

[42] M. B. Pinson and M. Z. Bazant, "Theory of SEI formation in rechargeable batteries: capacity fade, accelerated aging and lifetime prediction," *J. Electrochem. Soc.*, vol. 160, no. 2, p. A243, 2012.

[43] C. Chang, S. Wang, C. Tao, J. Jiang, Y. Jiang, and L. Wang, "An improvement of equivalent circuit model for state of health estimation of lithium-ion batteries based on mid-frequency and low-frequency electrochemical impedance spectroscopy," *Measurement*, vol. 202, p. 111795, 2022.

[44] Y. Zhou, G. Dong, Q. Tan, X. Han, C. Chen, and J. Wei, "State of health estimation for lithium-ion batteries using geometric impedance spectrum features and recurrent Gaussian process regression," *Energy*, vol. 262, p. 125514, 2023.

[45] X. Su, B. Sun, J. Wang, W. Zhang, S. Ma, X. He, and H. Ruan, "Fast capacity estimation for lithium-ion battery based on online identification of low-frequency electrochemical impedance spectroscopy and Gaussian process regression," *Appl. Energy*, vol. 322, p. 119516, 2022.

[46] L. Saunders, J. Wang, and U. Stimming, "Evaluating single-crystal and polycrystalline NMC811 electrodes in lithium-ion cells via non-destructive EIS alone," *J. Appl. Electrochem.*, vol. 52, no. 9, pp. 1305–1316, 2022.

[47] X. Zhao, Z. Wang, L. Eric, F. Gu, and A. D. Ball, "A pulse impedance technique for fast state of health estimation of EV lithium-ion batteries," in *Int. Conf. Effic. Perform. Eng. Netwk.*, Cham: Springer Nature Switzerland, Aug. 2022, pp. 220–233.